Phytoplankton community composition and photosynthetic physiology in the Australian sector of the Southern Ocean during the austral summer of 2010/2011

Shintaro Takao [a, b*] · Toru Hirawake [c] · Gen Hashida [d] · Hiroshi Sasaki [e] · Hiroshi Hattori [f] · Koji Suzuki [a, b, g]

[a] Graduate School of Environmental Science, Hokkaido University, North 10 West 5, Kita-ku, Sapporo, Hokkaido 060-0810, Japan

[b] Faculty of Environmental Earth Science, Hokkaido University, North 10 West 5, Kita-ku, Sapporo, Hokkaido 060-0810, Japan

[c] Faculty of Fisheries Sciences, Hokkaido University, 3-1-1 Minato-cho, Hakodate, Hokkaido 041-8611, Japan

[d] National Institute of Polar Research, 10-3 Midori-cho, Tachikawa, Tokyo 190-8518, Japan

[e] Department of Biological Sciences, Senshu University of Ishinomaki, Shinmito Minamisakai Ishinomaki, Miyagi 986-8580, Japan

[f] Department of Marine Sciences and Technology, Hokkaido Tokai University, Minamisawa, Minami-ku, Sapporo, Hokkaido 005-8601, Japan

[g] CREST, Japan Science and Technology Agency, North 10 West 5, Kita-ku, Sapporo, Hokkaido 060-0810, Japan

*Corresponding author. Tel.: +81 11 706 3026.

takao@ees.hokudai.ac.jp

Abstract Phytoplankton population dynamics play an important role in biogeochemical cycles in the Southern Ocean during austral summer. However, the relationship between phytoplankton community composition and primary productivity remains elusive in this region. We investigated the community composition and photosynthetic physiology of surface phytoplankton assemblages in the Australian sector of the Southern Ocean from Dec. 2010 to Jan. 2011. There were significant latitudinal variations in hydrographic and biological parameters along 110˚E and 140˚E. Surface (5 m) chlorophyll *a* (chl *a*) concentrations measured with high-performance liquid chromatography (HPLC) varied between 0.18 and 0.99 mg m^{-3}. The diatom contribution to the surface chl *a* biomass increased in the south, as estimated with algal chemotaxonomic pigment markers, while the contributions of haptophytes and chlorophytes decreased. In our photosynthesis-irradiance (*P*-*E*) curve experiment, the maximum photosynthetic rate normalized to chl *a* (P^*_{max}), initial slope (α^*), the maximum quantum yield of carbon fixation ($\Phi_{c\ max}$), and the photoinhibition index (β^*) were higher in the region where diatoms contributed > 50% to the chl *a* biomass. In addition, there were statistically significant correlations between the diatom contribution to the chl *a* biomass and the *P*–*E* parameters. These results suggested that the changes in the phytoplankton community composition, primarily in diatoms, could strongly affect photosynthetic physiology in the Australian sector of the Southern Ocean.

Keywords Phytoplankton community composition · Photosynthetic physiology · diatoms · FIRe fluorometry · Southern Ocean

Introduction

Phytoplankton primary productivity in the Southern Ocean plays an important role in the biogeochemical cycles, including the sequestration of atmospheric CO_2 (e.g., Takahashi et al. 2002; Sarmiento et al. 2004; McNeil et al. 2007). Previous field and remote sensing studies in the Southern Ocean have linked variations in primary productivity with dominant phytoplankton communities (e.g., Korb et al. 2005; Seeyave et al. 2007; Takao et al. 2012). However, it is not clear how vital the phytoplankton community composition is to controlling primary productivity in this region. Several studies have reported taxonomic differences in photosynthetic physiology among phytoplankton communities in the Southern Ocean (e.g., Claustre et al. 1997; Bracher et al. 1999). Because the Southern Ocean is one of the largest high-nutrient low-chlorophyll (HNLC) regions, the dominant phytoplankton community, photosynthetic physiology, and primary productivity could be controlled by iron availability (e.g., Martin et al. 1990; de Baar et al. 1995; Coale et al. 2004; Lance et al. 2007; Hiscock et al. 2008). In addition, phytoplankton productivity might be light-limited in the region due to the low irradiance caused by wind-induced vertical mixing, extensive cloud cover and seasonal ice (Mitchell et al. 1991; Nelson and Smith 1991). Recently, Alderkamp et al. (2010) investigated the influence of the high light part of the light cycle, which is induced by vertical mixing, on phytoplankton productivity in the Southern Ocean. This research suggests that phytoplankton growth

68 in the regions with mixing of deep layers could be controlled by photoinhibition
69 incurred during the high irradiance portion of the vertical mixing cycle, rather than the
70 by light limitation. A small number of studies have reported that the distribution of
71 dominant phytoplankton communities, primarily diatoms and the haptophyte
72 *Phaeocystis antarctica*, varies as a function of the mixed layer depth, i.e., light
73 availability, in the Ross Sea (Arrigo et al. 1999; Goffart et al. 2000) and the Indian
74 sector off East Antarctica (Wright and van den Enden 2000). In contrast, Smith and
75 Asper (2001) reported that there were no significant correlation between the distribution
76 of the dominant phytoplankton communities and the mixed layer depth in the Ross Sea.
77 Furthermore, there were no differences in the photosynthetic physiology between
78 diatoms and *P. antarctica* in the Ross Sea (van Hilst and Smith 2002). However, the
79 relationships among the phytoplankton community, photosynthetic physiology, and
80 primary productivity remain elusive in most of the Southern Ocean, excluding the Ross
81 Sea.

82 One of the useful methods for investigating the relationships between
83 irradiance and the photosynthetic rate of phytoplankton is a photosynthesis–irradiance
84 (*P–E*) curve experiment (Sakshaug et al. 1997), which provides information on the
85 physiological state of phytoplankton (Falkowski et al. 1992). In the Indian and
86 Australian sectors of the Southern Ocean, although several studies have examined the
87 spatiotemporal variability in phytoplankton's physiology of photosynthesis in terms of
88 *P–E* parameters (e.g., Hirawake et al. 2000; Strutton et al. 2000; Yoshikawa et al. 2007;

89 Westwood et al. 2010), notably few studies have investigated the relationship between
90 phytoplankton community composition and photosynthetic physiology. Recently, Uitz
91 et al. (2009) assessed the size-class-specific primary productivity in phytoplankton of
92 the Kerguelen Islands region of the Southern Ocean. However, these researchers used
93 physiological parameters derived from temperate and tropical oceanic regions, and
94 those could create errors in their estimates for the Southern Ocean. Nevertheless, a good
95 agreement between predicted and measured size-class-specific primary productivity was
96 observed for the bloom region, while their approach failed in the HNLC region that
97 accounts for a significant fraction of the Southern Ocean. Therefore, an extensive field
98 data set that includes the phytoplankton taxon- and/or size-class-specific photosynthetic
99 properties is needed to accurately assess the relationships among the dominant
100 phytoplankton communities, photosynthetic physiology, and primary productivity in the
101 Southern Ocean.
102 The objective of this study is to estimate the characteristics of phytoplankton
103 community composition and photosynthetic physiology in the Southern Ocean during
104 the austral summer of 2011. Initially, two fundamental questions were raised: (1) what
105 phytoplankton community was predominant in the region in situ? and (2) were there
106 differences among the dominant phytoplankton communities in photosynthetic
107 physiology?
108
109 **Materials and methods**

110

111 Sampling and hydrographic observations

112

113 Several observations were conducted in the Australian sector of the Southern
114 Ocean from 25 December 2010 to 19 January 2011 on board the TR/V *Umitaka-Maru*
115 (Tokyo University of Marine Science and Technology) as part of the project on
116 Responses of Antarctic Marine Ecosystems to global Environmental Changes with
117 carbonate systems (RAMEEC) of the Japanese Antarctic Research Expedition (JARE).
118 We established 23 sampling stations along 110˚E and 140˚E (Fig. 1). Seawater samples
119 were collected from 5 m in depth with acid-cleaned Teflon-coated Niskin bottles
120 attached to a CTD system (Falmouth Scientific Inc.) that measured seawater
121 temperature and salinity. At some stations, seawater samples were collected from a
122 continuous flow water source that drew from the bottom of the ship (approx. 5 m below
123 the sea surface), and vertical profiles of seawater temperature and salinity were
124 measured using a Seabird 911+ CTD sensor. The mixed layer depth at each station was
125 determined from individual profile based on a temperature difference (ΔT) criterion.
126 The criterion selected is a threshold value of temperature from a near-surface value at
127 10 m depth (ΔT = 0.2 ºC: de Boyer Montégut et al. 2004; Dong et al. 2008). Nutrients
128 (nitrite plus nitrate—hereafter denoted as nitrate, phosphate and silicate) were
129 determined in an onshore laboratory with a BRAN + LUEBBE auto-analyzer
130 (QuAAtro) following the manufacturer's protocol.

131

132 Phytoplankton pigment analysis by high-performance liquid chromatography

133

134 Seawater samples (1–2 liters) collected from the 5 m depth were filtered onto
135 25 mm Whatman GF/F filters under a gentle vacuum (< 0.013 MPa). The GF/F filters
136 were blotted with filter paper as much as possible after filtration. Similarly, seawater
137 samples (1.5–3 liters) were also filtered onto 25 mm nylon-mesh filters (20 μm in pore
138 size). The GF/F and nylon-mesh filters were stored in liquid nitrogen or in a
139 deep-freezer (-80°C) until analysis on land. The frozen filter was broken into small
140 pieces and soaked in 3 ml DMF (*N*, *N*-dimethylformamide) containing a known amount
141 of canthaxanthin as an internal standard. Next, the samples were sonicated with a
142 Branson SONIFIER Model 250 to break the cell walls. The suspension was extracted
143 for 2 h in the dark at -20°C. The extract was filtered through 0.45 μm PTFE filters to
144 remove fine particles. All procedures for the extraction were conducted under subdued
145 light to prevent the photo-degradation of the pigments. The 250-μl extract was mixed
146 with 250 μl 28 mM tetrabutylammonium acetate solution (pH 6.5), and 250 μl of the
147 mixture was injected into a Shimadzu CLASS-VP high-performance liquid
148 chromatography (HPLC) system with a Zorbax Eclips XDB-C8 column (4.6×150 mm,
149 3.5 μm particle size). A binary solvent system was employed for the HPLC pigment
150 analysis following Van Heukelem and Thomas (2001): solvent A (methanol: 28 mM
151 tetrabutylammonium acetate solution at pH 6.5, 70:30, v:v) and solvent B (methanol).

152 The flow rate was held constant at 1.2 ml min^{-1}. Pigment separation was made by the
153 linear gradient of 5 to 95% B in 22 min followed by an isocratic hold at 95% B for 8
154 min. The column temperature was kept at 60°C. Chlorophylls and carotenoids were
155 detected by absorbance using a Shimadzu photodiode array detector. The identification
156 of pigments are detailed in Suzuki et al. (2005).

157 In this study, the pigment data collected from the 5 m depth were interpreted
158 by the matrix factorization program CHEMTAX (Mackey et al. 1996) to estimate the
159 contributions of each algal class to the total chlorophyll *a* (chl *a*) biomass determined by
160 HPLC. For the CHEMTAX calculations, 23 pigment data were treated following the
161 methodology in Latasa (2007), with several seed values. The accessory pigment to chl *a*
162 ratios in Table 1 are based on the initial pigment ratios of Wright et al. (1996). A
163 dominant phytoplankton community was defined as having more than 50%
164 contributions to chl *a* biomass.

165

166 Flow cytometry

167

168 Duplicate seawater samples (2 ml) from the surface were preserved with
169 paraformaldehyde (0.2% final concentration), snap-frozen in liquid nitrogen, and stored
170 in a deep-freezer at -80°C until analysis on land. An EPICS flow cytometer (XL ADC
171 system, Beckman Coulter) equipped with a 15 mW air-cooled laser exciting at 488 nm
172 and the standard filter setup was used to enumerate ultraphytoplankton (< 5 μm in size).

Prior to analysis, samples were thawed and then drawn through 35 μm nylon-mesh-capped Falcon cell strainer (Becton-Dickinson) to remove larger cells. For the enumeration of ultraphytoplankton, a known volume of Flow-Count fluorospheres (Beckman Coulter) and 2.0 μm Fluoresbrite YG beads (Poly Sciences) were added to each sample. The details of flow cytometric analysis are described in Suzuki et al. (2005).

Photosynthesis–irradiance (*P*–*E*) curve experiment

Seawater samples were dispensed into a set of ten 275 mL acid-cleaned polystyrene bottles, and all of the bottles were inoculated with a solution of $NaH^{13}CO_3$ (99 atom% ^{13}C, Shoko Co., Ltd.), which was equivalent to approximately 10% of dissolved inorganic carbon (DIC) in the seawater. Incubations were carried out for 2 h at 10 irradiance levels from approximately 10 to 2260 μmol photons m^{-2} s^{-1} in a bench-top incubator. The incubator was cooled to surface seawater temperature with a temperature-controlled water circulator. The details of incubation and sample analysis were described in Isada et al. (2009). In this study, however, to determine the particulate organic carbon (POC) and the ^{13}C abundance of the sample, a mass spectrometer (DELTA V Plus, Thermo Fisher Scientific Inc.) with an in-line elemental analyzer (Flash EA1112, Thermo Fisher Scientific Inc.) was used. The amount of DIC in seawater was determined with a coulometer (Model 5012, UIC) following the

methodology in DOE (1994). Photosynthetic rates were determined following the method of Hama et al. (1983) and normalized to the chl *a* concentration measured with HPLC (see above). Photosynthesis–irradiance (*P*–*E*) parameters were obtained from the photoinhibition model of Platt et al. (1980) as follows:

$$P^* = P_s^*[1 - \exp(-\alpha^* \cdot E/P_s^*)] \cdot \exp(-\beta^* \cdot E/P_s^*) \quad (1)$$

$$P_{max}^* = P_s^* \cdot [\alpha^*/(\alpha^* + \beta^*)] \cdot [\beta^*/(\alpha^* + \beta^*)]^{\beta^*/\alpha^*} \quad (2)$$

where subscription * denotes a normalized chl *a* concentration, P^* [mg C (mg chl *a*)$^{-1}$ h^{-1}] is the observed photosynthetic rate, P^*_s [mg C (mg chl *a*)$^{-1}$ h^{-1}] is the theoretical maximum photosynthetic rate with no photoinhibition (i.e., $\beta^* = 0$), α^* {[mg C (mg chl *a*)$^{-1}$ h^{-1}] (µmol photons m^{-2} s^{-1})$^{-1}$} is the initial slope, E (µmol photons m^{-2} s^{-1}) is the irradiance, β^* {[mg C (mg chl *a*)$^{-1}$ h^{-1}] (µmol photons m^{-2} s^{-1})$^{-1}$} is the photoinhibition index, and P^*_{max} [mg C (mg chl *a*)$^{-1}$ h^{-1}] is the maximum photosynthetic rate. The light saturation index, E_k, is defined by P^*_{max} and α^* (i.e., $E_k = P^*_{max}/\alpha^*$).

The maximum quantum yield of carbon fixation ($\Phi_{c\,max}$, mol C mol photons^{-1}) was derived from the following equation:

$$\Phi_{c\,max} = 0.0231\ \alpha^*/\bar{a}_\varphi^* \quad (3)$$

where 0.0231 converts milligrams of carbon on moles, µmol photons to moles, and hours to seconds, and $\bar{a}^*_\varphi$ is the mean chl *a*-specific absorption coefficient of phytoplankton (see below). The chl *a*-specific absorption spectra of phytoplankton, $a^*_\varphi(\lambda)$, were measured using the glass fiber technique of Kishino et al. (1985). The optical density (OD) of all particles on the filter was measured between 350 and 750 nm

215 with 1 nm intervals using a MPS-2450 spectrophotometer (Shimadzu). A blank filter
216 wetted with filtered seawater was used as a reference (Suzuki et al. 1998). The OD at
217 750 nm was subtracted from all wavelengths as a scattering correction assuming the
218 lack of the absorption at 750 nm. The filter was subsequently soaked in methanol to
219 extract phytoplankton pigments (Kishino et al. 1985), and the OD of non-algal particles
220 (NAPs) was re-measured with the same manner as the OD of all particles mentioned
221 above. The absorption coefficient of all of the suspended particles and NAPs were
222 corrected for the path length amplification on the glass fiber filters using the equation in
223 Cleveland and Weidemann (1993). The absorption coefficient of phytoplankton, $a_{\varphi}(\lambda)$,
224 was calculated as the difference between the values before and after pigment extraction.
225 The mean chl *a*-specific absorption coefficient of phytoplankton, $\bar{a}^*_{\varphi}$, was weighted
226 with the spectral irradiance of an incubator lamp from 400 to 700 nm to correct for the
227 spectral characteristics of an incubator lamp source (Cota et al. 1994):

228 $$\bar{a}^*_{\varphi} = \int_{400}^{700} a^*_{\varphi}(\lambda) \cdot E_{\mathrm{NL}}(\lambda) d\lambda / \int_{400}^{700} E_{\mathrm{NL}}(\lambda) d\lambda \quad (4)$$

229 where $E_{\mathrm{NL}}(\lambda)$ is the normalized spectral irradiance of an incubator lamp and was
230 estimated as follows:

231 $$E_{\mathrm{NL}}(\lambda) = E_{\mathrm{L}}(\lambda) / \int_{\lambda} E_{\mathrm{L}}(\lambda) d\lambda \quad (5)$$

232 where $E_{\mathrm{L}}(\lambda)$ is an incubator's lamp spectrum.

233

234 Fluorescence induction and relaxation (FIRe) fluorometry

235

Seawater samples were collected from the same seawater as the phytoplankton pigment samples. To open the reaction centers, the sample was acclimated in the dark for at least 30 min in an incubator, which was adjusted to the in situ seawater temperature. Variable fluorescence of phytoplankton was measured with a Fluorescence Induction and Relaxation (FIRe) fluorometer (Satlantic Inc.) in a dark room (Gorbunov et al. 1999). The FIRe fluorometer was equipped with blue (455 nm with 60 nm bandwidth) and green (540 nm with 60 nm bandwidth) light-emitted diodes (LED). The FIRe protocol involved a strong flash of saturating blue and green that initiated a rise in fluorescence in vivo from the initial value (F_0) to the maximum value (F_m) in a strong short pulse of 80 μs duration (i.e., single-turnover flash). This change in fluorescence ($F_v = F_m - F_0$) is associated with absorption and utilization energy in photosynthesis and is normalized to F_m to deduce the photochemical quantum efficiency (F_v/F_m) of phytoplankton photosystem II (Kolber et al. 1988). The functional absorption cross-section of photosystem II (σ_{PSII}, $\times 10^{-20}$ m^2 $quanta^{-1}$) is derived from the slope where fluorescence increases from F_0 to F_m against the cumulated light energy provided with the fluorometer. Although the photosystem II action spectrum for cyanobacteria is typically much lower in blue light than in green one (e.g., Suggett et al. 2009), cyanobacteria were present in relatively low abundances in this study area (e.g., Marchant et al. 1987; Odate and Fukuchi 1995; Zubkov et al. 1998; Fouilland et al. 1999). Thus, only the blue (i.e., 455 nm) saturating light was used in this study. Triplicate samples were measured with up to 50 iterations per sample. For all analyses,

257 a 0.45-μm filtered seawater sample was used as a blank. The fluorescence data were
258 processed with the MATLAB-based program fireworx developed by Audrey Barnett
259 (Dalhousie Univ.) to obtain F_v/F_m and σ_{PSII} values.
260
261 Light microscopy
262
263 Seawater samples (500 ml) collected from the surface were preserved with
264 4% Lugol's iodine solution. The samples were concentrated using Utermöhl chambers
265 (HYDRO-BIOS Apparatebau GmbH) and analyzed with an inverted microscope
266 (BIOREVO BZ-9000, Keyence). Phytoplankton cells were identified following Tomas
267 (1997) and Scott and Marchant (2005).
268
269 Light availability
270
271 At 10 out of 23 stations, the underwater downwelling irradiance, $E_d(\lambda, z)$, was
272 obtained using a PRR-800 spectroradiometer (Biospherical Instruments Inc.) with a
273 reference of PRR-810, which monitored the incident irradiance just above the sea
274 surface. The PRR-800 has 17 wavelengths between 380 and 765 nm and was deployed
275 on the sunny side of the ship to minimize its shadow. The value of $E_d(\lambda, z)$ at just below
276 the sea surface was obtained by extrapolation of logarithm-transformed data from 1 to 4
277 m. Photosynthetic active radiation (PAR) was calculated at each depth, integrating $E_d(\lambda,$

z) over 400–700 nm. The attenuation of PAR in a water column, K_d (PAR), was determined as the slope of least-squares regression fit to logarithm-transformed E_d (PAR) as a function of depth. If PRR-800 data were unavailable, K_d (PAR) was estimated using an empirical relationship between in situ K_d (PAR) and surface fluorometric-derived chl *a* concentrations in the Southern Ocean (Venables and Moore, 2010):

$$K_d(\mathrm{PAR}) = 0.05 + 0.057 \text{ chl } a \text{ (fluorometry)}^{0.58} \quad (6)$$

where chl *a* (fluorometry) is chl *a* concentration at 5 m depth as derived using the non-acidification method of Welschmeyer (1994). K_d (PAR) was used to calculate euphotic depth and total daily PAR in the upper mixed layer as described in Alderkamp et al. (2010). In this study, however, to estimate total daily surface PAR, the moderate-resolution imaging spectroradiometer (MODIS)/Aqua 8-day composite images (9 km resolution) of the Distributed Active Archive Center (DAAC)/Goddard Space Flight Center (GSFC), NASA were used.

Satellite data processing

To investigate the temporal and spatial changes in chl *a* concentration before and after our cruise, the distributions of chl *a* concentration as determined from MODIS/Aqua 8-day composite images for the period from August 2010 to March 2011 were used. To maximize available data, we averaged the each 8-day composite image

299 with 3 × 3 pixels (i.e., 27 km × 27 km) resolution.

300

301 **Results**

302

303 Hydrography and phytoplankton abundance

304

305 Hydrographic conditions at each station during the cruise are listed in Table 2.
306 Along the 110˚E transect, the sea surface temperature (SST) and salinity (SSS) tended
307 to decrease in the south and ranged from 1.3 to 15.9°C and from 33.3 to 35.3,
308 respectively. Surface macronutrient (nitrate, phosphate, and silicate) levels also tended
309 to increase toward the south. Although surface nitrate and phosphate were present along
310 the 110˚E transect, surface silicate was depleted between Stations (Stn.) C01 and C02
311 (< 0.17 μmol L^{-1}) (Fig. 1 and Table 2). However, an ample amount of silicate (> 20
312 μmol L^{-1}) remained at stations south of Stn. C04 (55˚S) as did the other macronutrients.
313 Along the 140˚E transect, SST decreased toward south (0.7−10.0°C) as with the 110˚E
314 transect. Although SSS, nitrate, and phosphate were relatively constant, silicate
315 drastically decreased between Stns. D12 and D13 (i.e., from 20.6 to 3.0 μmol L^{-1}). In
316 the results of Wilcoxon rank sum test, no significant difference in hydrographic
317 conditions was observed between the two transects during the cruise (SST: p = 0.15,
318 SSS: p = 0.10, nitrate: p = 0.08, phosphate: p = 0.12, silicate: p = 0.57).
319 In both transects, there were relatively high abundances of *Synechococcus*

320 measured with the flow cytometry only at Stns. C01 and S02 (> 20.0 × 10^3 cells ml^{-1})
321 (Fig. 1 and Table 2). Except at those stations, *Synechococcus* concentrations were
322 relatively low (< 3.0 × 10^3 cells ml^{-1}). The surface chl *a* concentrations measured with
323 HPLC varied from 0.18 to 0.99 mg m^{-3}, and no significant difference was observed
324 between the transects (Wilcoxon rank sum test, $p = 0.48$). The highest chl *a* value was
325 observed in water with low temperature and salinity (Stn. S09), where micro-sized (>
326 20 μm) phytoplankton accounted for 25% of the total chl *a* biomass. Overall, the
327 contribution of micro-sized phytoplankton to the total chl *a* biomass was relatively low
328 (< 50%), and nano- and pico-sized (< 20 μm) phytoplankton dominated the
329 phytoplankton assemblages during our cruise.
330
331 Phytoplankton community composition as estimated by CHEMTAX
332
333 Figure 2 shows the contributions of each algal class to the total chl *a* biomass
334 estimated by CHEMTAX. Along the 110˚E transect, haptophytes type6 (presumably
335 coccolithophores *Emiliania huxleyi*; Zapata et al., 2004), haptophytes type8
336 (presumably *P. antarctica*; Zapata et al., 2004), and chlorophytes were the major algal
337 groups between Stns. C01 and C03 (Fig. 2a). The relatively high contributions of
338 cyanobacteria to the chl *a* biomass were only found at Stns. C01 and S02 (19% and 12%,
339 respectively). Although diatoms were the minor constituents between Stns. C01 and
340 C03, they contributed to the chl *a* biomass with > 50% between Stns. C04 and C10.

341 Along the 140˚E transect, diatoms contributed to the chl *a* biomass with > 50% except
342 Stn. D15 (Fig. 2b). At Stn. D15, diatoms contributed to the chl *a* biomass with 44%,
343 haptophytes (type6 and type8) and chlorophytes accounted for 56% of the total chl *a*
344 biomass. As a result, the area south of 55˚S was defined as a diatom-dominated area in
345 this study (i.e., Stns. C04, C05, C06, S09, C08, C10, C17, S15, D07, D08, D10, D12,
346 D13, S21, and D14). Along both transects, dinoflagellates, cryptophytes, and
347 prasinophytes were minor algal groups, and their contributions to the chl *a* biomass
348 were < 14%.
349
350 Light availability in the upper mixed layer
351
352 There were significant latitudinal variations in the depth of upper mixed layer
353 (z_{UML}) and euphotic zone (z_{eu}), incident surface PAR, and total daily PAR in the upper
354 mixed layer (E_{UML}) along the 110˚E and 140˚E transects (Fig. 3). Along the 110˚E
355 transect, z_{UML} ranged from 11 to 92 m, and the shallowest values were observed at Stns.
356 C08, C10, and C17 (Fig. 3a). Along the 140˚E transect, z_{UML} ranged from 13 to 68 m
357 (Fig. 3b), and no significant difference was observed relative to the 110˚E transects
358 (Wilcoxon rank sum test, p = 1.0). In general, z_{UML} was shallower than z_{eu} along the
359 both transects with a few exceptions. Incident surface PAR tended to decrease in the
360 south along the 110˚E transect, while relatively high E_{UML} values (> 10 mol photons m^{-2}
361 d^{-1}) were also observed in the south due to the shallow z_{UML} (Fig. 3c). Along the 140˚E

362 transect, both incident surface PAR and E_{UML} were similar to values along the 110˚E
363 transect (Fig. 3d), and no significant differences in the both parameters were observed
364 between the two transects (Wilcoxon rank sum test, PAR: $p = 0.57$, E_{UML}: $p = 0.74$).
365 There was no significantly correlation between total daily PAR in the upper mixed layer
366 (E_{UML}) and surface chl *a* concentration (Nonparametric Kendall's rank correlation, $p =$
367 0.26).

368 The value of z_{UML} in the diatom-dominated and non-diatom-dominated areas
369 varied from 11 to 92 m and from 13 to 84 m, respectively (Figs. 2 and 3). In the
370 diatom-dominated area, the value of E_{UML} varied from 4.0 to 22.7 mol photons m^{-2} d^{-1}.
371 While the minimum value in the non-diatom-dominated area was higher than that in the
372 diatom-dominated area (i.e., 8.8 mol photons m^{-2} d^{-1}), the maximum value was almost
373 same (i.e., 23.0 mol photons m^{-2} d^{-1}). In the results of Wilcoxon rank sum test, no
374 significant differences were observed in z_{UML} and E_{UML} between the diatom-dominated
375 and non-diatom-dominated areas (z_{UML}: $p = 0.86$, E_{UML}: $p = 0.12$). Furthermore, there
376 were no statistically significant correlations between the diatom contribution to the chl *a*
377 biomass and z_{UML} as well as E_{UML} (Nonparametric Kendall's rank correlation, z_{UML}: $p =$
378 0.19, E_{UML}: $p = 0.92$).

379

380 *P*–*E* parameters

381

382 In the diatom-dominated area, significantly higher values of the maximum

383 photosynthetic rate normalized to chl *a* (P^*_{max}), initial slope (α^*), photoinhibition index
384 (β^*), and maximum quantum yield of carbon fixation ($\Phi_{c\,max}$) were observed compared
385 with the non-diatom-dominated area (Wilcoxon rank sum test, P^*_{max}: $p < 0.05$, α^*: $p <$
386 0.05, β^*: $p < 0.05$, $\Phi_{c\,max}$: $p < 0.01$). The value of P^*_{max} in the diatom-dominated and
387 non-diatom-dominated areas varied from 0.95 to 1.87 mg C (mg chl *a*)$^{-1}$ h^{-1} and from
388 0.74 to 1.26 mg C (mg chl *a*)$^{-1}$ h^{-1}, respectively (Fig. 4a). In this study, α^* values
389 increased toward the south (Fig. 4b). The values of α^* in the diatom-dominated area
390 varied from 0.0069 to 0.0134 mg C (mg chl *a*)$^{-1}$ h^{-1} (μmol photons m^{-2} s^{-1})$^{-1}$, while the
391 maximum value in the non-diatom-dominated area was 0.0078 mg C (mg chl *a*)$^{-1}$ h^{-1}
392 (μmol photons m^{-2} s^{-1})$^{-1}$. As for α^*, β^* also increased toward the south (Fig. 4c). The
393 values of $\Phi_{c\,max}$ in the diatom-dominated area varied from 0.009 to 0.016 mol C (mol
394 photons)$^{-1}$, and the minimum value was higher than the maximum value (i.e., 0.007 mol
395 C (mol photons)$^{-1}$) observed in the non-diatom-dominated area (Fig. 4d). The values of
396 $\bar{a}^*_{\varphi}$ in the diatom-dominated and non-diatom-dominated areas varied from 0.017 to
397 0.030 m^2 (mg chl *a*)$^{-1}$ and from 0.021 to 0.035 m^2 (mg chl *a*)$^{-1}$, respectively (Fig. 4e).
398 Relatively high E_K values were observed at Stns. C01 and D15 in the
399 non-diatom-dominated area (Fig. 4f). However, no significant differences were
400 observed in $\bar{a}^*_{\varphi}$ and E_K between the diatom-dominated and non-diatom-dominated areas
401 (Wilcoxon rank sum test, $\bar{a}^*_{\varphi}$: $p = 0.16$, E_K: $p = 0.31$).
402
403 Variable fluorescence of phytoplankton

404

405 The relationship between the photochemical quantum efficiency (F_v/F_m) and
406 the functional absorption cross-section (σ_{PSII}) of photosystem II for the phytoplankton
407 community at 5 m along the 110˚E and 140˚E transects are shown in Figure 5. Along
408 the transects, F_v/F_m values were consistently low (≦ 0.25), and no significant difference
409 in F_v/F_m was observed between the diatom-dominated and non-diatom-dominated areas
410 (Wilcoxon rank sum test, $p = 0.21$). The values of σ_{PSII} varied from 141 to 513 $\times 10^{-20}$
411 m^2 $quanta^{-1}$, and no significant difference in σ_{PSII} was observed (Wilcoxon rank sum test,
412 $p = 0.68$). There was no statistically significant correlation between the values of F_v/F_m
413 and σ_{PSII} in the transects (Nonparametric Kendall's rank correlation, $p = 0.21$).

414

415 Temporal and spatial changes in chl *a* concentration derived from satellite ocean-color

416

417 Figure 6 shows temporal and spatial changes in the distributions of
418 satellite-derived chl *a* concentration (chl_{sat}) in the study area from August 2010 to
419 March 2011 along 110˚E and 140˚E. Along the 110˚E transect, chl_{sat} in the area between
420 Stns. C02 and C03 were relatively high before our cruise (i.e., from October to
421 November) and decreased significantly from December to March (Fig. 6a). However,
422 there were relatively constant chl_{sat} in the area between Stns. C03 and C05 until March.
423 In the area south of Stn. C06, clear blooming events ($chl_{sat} > 1$ mg m^{-3}) occurred before
424 and after our cruise. Along the 140˚E transect, chl_{sat} in the area north of Stn. D12 were

425 relatively high before our cruise and decreased after our cruise (Fig. 6b). In the area
426 south of Stn. D10, clear blooming events occurred after our cruise.
427
428 **Discussion**
429
430 Latitudinal changes in the abundance and community composition of phytoplankton
431
432 There were considerable changes in the abundance and community
433 composition of phytoplankton with latitude in the Australian sector of the Southern
434 Ocean during the austral summer of 2010/2011. The contributions of each algal class to
435 the total chl *a* biomass estimated by CHEMTAX drastically changed toward south,
436 particularly along the 110˚E transect (Fig. 2). Although the contribution of
437 cyanobacteria to the chl *a* biomass and the cell densities of *Synechococcus* measured
438 with flow cytometry were relatively high at Stns. C01 and S02, a dramatic decrease in
439 both the contributions and the cell concentrations occurred to the south of those stations
440 (Table 2 and Fig. 2a). As a result, cyanobacteria were minor algal groups in most of the
441 study area. Those latitudinal patterns were consistent with the previous reports for the
442 Southern Ocean (e.g., Marchant et al. 1987; Odate and Fukuchi 1995; Wright et al.
443 1996; Zubkov et al. 1998; Fouilland et al. 1999). Along the 110˚E transect, haptophytes
444 type6, haptophytes type8, and chlorophytes were the major algal groups in the area
445 north of 50˚S, while diatoms contributed to the chl *a* biomass with more than 50% in the

area south of 55˚S. Those latitudinal gradients in each algal class were consistent with the previous CHEMTAX interpretations of HPLC pigment data in the Australian sector of the Southern Ocean (e.g., Wright et al. 1996).

Since the Southern Ocean is a HNLC region, the abundance and community composition of phytoplankton were thought to be mainly controlled by availability of light (e.g., Mitchell et al. 1991; Nelson and Smith 1991; Arrigo et al. 1999; Goffart et al. 2000; Wright and van den Enden 2000) and iron (e.g., de Baar et al. 1995; Boyd et al. 2000; Lance et al. 2007) from the perspective of bottom-up control. A shallow mixed layer leads to a higher E_{UML} that stimulates phytoplankton growth (Mitchell et al. 1991). During our cruise, most z_{UML} were shallower than z_{eu} (Fig. 3). However, there was no significantly correlation between E_{UML} and surface chl *a* concentration. Previous studies in the Southern Ocean have reported that the distribution of dominant phytoplankton communities varies as a function of the mixed layer depth (Arrigo et al. 1999; Goffart et al. 2000; Wright and van den Enden 2000), while there were no significant correlations between the diatom contribution to the chl *a* biomass and z_{UML} as well as E_{UML} in this study. These results suggested that latitudinal changes in the abundance and community composition of phytoplankton might not be light limited during our cruise.

The surface macronutrient levels for all substances except silicate (Table 2) were generally higher than the mean half-saturation constant, K_s, of each macronutrient for diatoms (Sarthou et al. 2005) and for haptophytes *phaeocystis* (Schoemann et al. 2005), indicating that nitrate and phosphate were not the dominant factors controlling

467 latitudinal changes in the algal photosynthetic physiological condition. Nelson and
468 Tréguer (1992) reported that silicate was a limiting factor the growth of diatoms and/or
469 silicoflagellates at the stations where silicate was less than 5 μmol L^{-1} at the time of
470 sampling. Along the 140˚E transect, the surface silicate was less than 5 μmol L^{-1} at Stns.
471 D13, S21, D14, and D15 (Table 2), while diatoms contributed > 50% to the chl *a*
472 biomass except at Stn. D15 (Fig. 2b). According to the light microscopy, the
473 chain-forming pennate diatom *Fragilariopsis kerguelensis* was also present at Stns. D14
474 and D15 (Fig. 7). Satellite-derived chl *a* concentrations were relatively high in the area
475 north of Stn. D12 before our cruise (Fig. 6b). These results suggested that the low
476 silicate level in the area north of Stn. D13 could be due to the consumption by diatoms
477 and/or silicoflagellates.

478 It is known that iron availability was very low in the Australian sector of the
479 Southern Ocean (e.g., Sohrin et al. 2000; Bowie et al. 2004; Sedwick et al. 2008). Iron
480 and nitrate limitations lead to a decrease in F_v/F_m of algal photosystem II (e.g., Greene
481 et al. 1992; Kolber et al. 1994; Boyd and Abraham 2001; Suzuki et al. 2002). Although
482 the surface nitrate was abundant in this study (Table 2), the F_v/F_m values were
483 considerably lower (≦ 0.25: Fig. 5) than the empirical maximum (approximately 0.65:
484 Falkowski et al. 1994). These results suggested that the abundance of phytoplankton in
485 this area could be controlled by iron availability. However, chl *a* concentrations were
486 relatively high in the southern part of the transects (Table 2). The chl *a* concentration
487 derived from satellite ocean-color was also relatively high before our cruise in the

488 southern part of the transects where sea ice covered until October (Fig. 6). Sea ice
489 melting caused the changes in the mixed layer depth (e.g., Mitchell and Holm-Hansen
490 1991) and iron availability (e.g., Lannuzel et al. 2007), affecting phytoplankton
491 abundance (e.g., Boyd et al. 2000). Thus, relatively high chl *a* concentration in the
492 region might be caused by improved growth conditions before our cruise.

493 The observed values of F_v/F_m in this study (Fig. 5) was comparable to the
494 ranges reported outside an iron enriched patch during SOIREE, a past in situ iron
495 enrichment experiment in the Australian sector of the Southern Ocean (Boyd and
496 Abraham 2001). However, the ranges of the two parameters in this study were very
497 narrow compared to other previous studies in the Mertz Glacier Region of East
498 Antarctica (Vaillancourt et al. 2003) and in the vicinity of the Crozet Plateau (Moore et
499 al. 2007). These studies reported that values of F_v/F_m and σ_{PSII} were highly correlated
500 (Vaillancourt et al. 2003; Moore et al. 2007). On the other hand, there was no
501 statistically significant correlation between the two parameters in this study (Fig. 5).
502 Suggett et al. (2009) reported that F_v/F_m and σ_{PSII} varied principally with broad-scale
503 changes in community structure, and the slope of the F_v/F_m versus σ_{PSII} relationship was
504 much steeper for cyanobacteria than it is for diatoms and haptophytes. However, since
505 cyanobacteria were minor algal groups in this study areas, the absence of relationship
506 between F_v/F_m and σ_{PSII} might be caused by other reasons. Moore et al. (2007) indicated
507 that responses of the variable fluorescence parameters (i.e., F_v/F_m and σ_{PSII}) to a drop in
508 iron availability may be more varied in a condition approximating steady-state

509 limitation occurs, although rapid changes in the parameters tend to follow increased iron
510 availability to a starved population. Thus, further studies are needed to examine the
511 relationships between the variable fluorescence parameters and phytoplankton
512 community compositions in as the Southern Ocean, where phytoplankton growth is
513 often limited by low iron availability.
514
515 Differences in photosynthetic physiology between the dominant phytoplankton
516 communities
517
518 Significant higher *P*–*E* parameters (P^*_{max}, α^*, β^*, and $\Phi_{c\ max}$) in the
519 diatom-dominated area were observed (Figs. 4a-d). It is well known that P^*_{max} is
520 dependent on temperature because it is controlled by the activity of enzymes such as
521 RuBisCO (Sukenik et al. 1987; MacIntyre and Geider 1996). Although high
522 temperatures increase enzymatic activity and carbon fixation (Davison 1991; Sakshaug
523 et al. 1997), the seawater temperature in the diatom-dominated area was significantly
524 lower than that in the non-diatom-dominated area (Wilcoxon rank sum test, $p < 0.05$).
525 These results suggested that factors other than temperature may play a more important
526 role in the control of P^*_{max}.
527 Several studies have reported a significant effect of irradiance levels on the
528 photosynthetic physiology of phytoplankton in the Southern Ocean (e.g., Bracher et al.
529 1999; van Hilst and Smith 2002). In the Atlantic sector, Bracher et al. (1999) reported

that beyond frontal zones, P^*_{max} values at the 1% irradiance level were significantly higher than those at the surface (i.e., 100% irradiance level). However, in the Ross Sea, no differences existed between P^*_{max} values at the 1% irradiance level and those at the 50% irradiance level, while significant differences in α^* and E_k were observed between the two irradiance levels (van Hilst and Smith 2002). In this study, although significant higher P^*_{max}, α^*, β^*, and $\Phi_{c\ max}$ were observed in the diatom-dominated area, no significant differences were observed in z_{UML} and E_{UML} between the diatom-dominated and non-diatom-dominated areas. Indeed, no significant difference was observed in E_K between the diatom-dominated and non-diatom-dominated areas. Thus, the differences in photosynthetic physiology between the diatom-dominated and non-diatom-dominated areas may have resulted from factors other than light availability.

In the past in situ iron enrichment experiments, several studies reported photosynthetic physiology of phytoplankton communities in HNLC regions was affected by changes in iron availability (e.g., Gervais et al. 2002; Hiscock et al. 2008; Suzuki et al. 2009). In the Southern Ocean during EisenEx (Gervais et al. 2002) and SoFeX (Hiscock et al. 2008), α^* became higher inside the iron enriched patch, whereas there was no difference in P^*_{max} between inside and outside the iron patch. However, in the Western Subarctic Gyre (WSG) during SEEDS-II (Suzuki et al. 2009), higher P^*_{max} values were observed inside the iron enriched patch, but α^* was little affected by the iron additions. Although several studies reported F_v/F_m increased inside the iron patch, temporal changes in the P–E parameters and F_v/F_m were not always correspond with

each other (Gervais et al. 2002; Suzuki et al. 2009). In this study, the F_v/F_m values in the diatom-dominated and non-diatom-dominated areas were considerably low, while significant higher P^*_{max}, α^*, β^*, and $\Phi_{c\ max}$ in the diatom-dominated area were observed. These results suggested that changes in the *P*–*E* parameters might not always be related to absolute values of F_v/F_m.

In this study, there was strong covariation between the P^*_{max} and α^* (Table 3), indicating E_k-independent variability (Behrenfeld et al. 2004). Covariability in P^*_{max} and α^* was frequently observed in the Southern Ocean (Tilzer et al. 1986; Claustre et al. 1997; Moline et al. 1998; Moore et al. 2007). Photosynthetic process is divided into two processes, i.e., the photosynthetic electron transfer (PET) process (e.g., light-harvesting and reductant production) and downstream processes of PET (e.g., carbon fixation). The *P*–*E* parameters were related to both processes (i.e., PET and the downstream processes of PET), whereas the variable fluorescence parameters measured with FIRe fluorometer (i.e., F_v/F_m and σ_{PSII}) were sololy related to the PET process. Comparing these parameters, there were no statistically significant correlations between F_v/F_m or σ_{PSII} and most of the *P*–*E* parameters, except for β^* (Table 3), indicating that the PET processes did not play important roles in the changes in most of the *P*–*E* parameters. Previous studies also showed the importance of the downstream processes of PET for the E_k-independent variability (Behrenfeld et al. 2004; Yoshie et al. 2010). Although several factors have been suggested as drivers for the E_k-independent variability (Behrenfeld et al. 2004), Claustre et al. (1997) suggested that changes in phytoplankton

572 community composition were largely responsible for the E_k-independent variability in
573 the Antarctic Peninsula shelf. However, the mechanism of the E_k-independent
574 variability is largely unresolved. Therefore, further studies are needed to clarify the
575 factors controlling the E_k-independent variability in the Southern Ocean.

576 The observed values of *P*–*E* parameters in this study (Fig. 4) were
577 comparable to the ranges previously reported for the Australian sector of the Southern
578 Ocean during austral summer (Hirawake et al. 2000; Yoshikawa et al. 2007).
579 Yoshikawa et al. (2007) and Hirawake et al. (2000) reported that P^*_{max}, α^*, and $\Phi_{c\ max}$
580 tended to be high toward south at approximately 140˚E in the Southern Ocean during
581 the austral summer, and their results were consistent with this study. However, their
582 studies did not examine phytoplankton community composition. On the other hand,
583 Bracher et al. (1999) reported that P^*_{max} and $\Phi_{c\ max}$ tended to be high in the polar front
584 (PF) positioned approximately 50˚S and low in the marginal ice zone (MIZ)
585 approximately 64˚S in the Atlantic sector of the Southern Ocean during austral summer.
586 Although the latitudinal pattern reported by Bracher et al. (1999) showed an opposite
587 trend in this study, Bracher et al. (1999) reported that diatoms dominated the
588 phytoplankton community in the PF and the haptophyte *Phaeocystis* sp. dominated in
589 the MIZ. As a result, both P^*_{max} and $\Phi_{c\ max}$ in the diatom-dominated area (i.e., the PF)
590 were higher than those observed in the non-diatom-dominated area (i.e., the MIZ), as
591 found in this study. In the Antarctic coastal waters, Claustre et al. (1997) also reported
592 that the depth-averaged values of P^*_{max} and α^* for diatoms were higher than those for

593 cryptophytes, although cryptophytes were minor constituents in this study (Fig. 2). To
594 assess the effect of the phytoplankton community composition on changes in the *P*–*E*
595 parameters, the relationships between the diatom contribution to the chl *a* biomass and
596 the *P*–*E* parameters were examined (Table 3). There were statistically significant
597 correlations between the diatom contribution to the chl *a* biomass and most of the *P*–*E*
598 parameters, except for α^* and E_k. Thus, latitudinal changes in the *P*–*E* parameters could
599 be accompanied by changes in the phytoplankton community composition, mainly
600 diatoms. Although this study primarily focused on the community composition and
601 photosynthetic physiology of phytoplankton at the sea surface, vertical changes in the
602 distribution and abundance of phytoplankton communities were found in the Southern
603 Ocean (e.g., Wright and van den Enden 2000; Wright et al. 2010; de Salas et al. 2011).
604 Therefore, further studies are needed to examine the responses of the community
605 composition and photophysiology of phytoplankton assemblages to vertical changes in
606 the underwater light field in the Southern Ocean.
607
608 **Acknowledgments**
609
610 We are grateful to the captain and crew of the TR/V *Umitaka-Maru*, Dr. M.
611 Moteki (Tokyo University of Marine Science and Technology), and many other
612 colleagues on board for their assistance in collecting samples during cruises. We thank
613 Dr. T. Odate (National Institute of Polar Research) for giving a chance to join the JARE

614 RAMEEC (Responses of Antarctic Marine Ecosystems to global Environmental
615 Changes with Carbonate systems) project. We also thank the Distributed Active
616 Archive Center (DAAC) at the Goddard Space Flight Center (GSFC) for the production
617 and distribution of satellite data. We appreciate the editor, Dr. A-C. Alderkamp, and
618 two anonymous reviewers for providing valuable comments that improved the
619 manuscript significantly. This work was supported in part by the Japan Society for the
620 Promotion of Science (JSPS), the JARE RAMEEC project, and the JAXA GCOM-C
621 RA4 (JX-PSPC-381949).

622 **References**

623

624 Alderkamp A-C, de Baar HJW, Visser RJW, Arrigo KR (2010) Can photoinhibition
625 control phytoplankton abundance in deeply mixed water columns of the Southern
626 Ocean? Limnol Oceanogr 55:248–1264
627 Arrigo KR, Robinson DH, Worthen DL, Dunbar RB, DiTullio GR, van Woert M,
628 Lizotte MP (1999) Phytoplankton community structure and the drawdown of
629 nutrients and CO_2 in the Southern Ocean. Science 283:365–367
630 Behrenfeld MJ, Prasil O, Babin M, Bruyant F (2004) In search of physiological basis
631 for covariations in light-limited and light-saturated photosynthesis. J Phycol 40:
632 4-25
633 Bowie AR, Sedwick PN, Worsfold PJ (2004) Analytical intercomparison between flow
634 injection–chemiluminescence and flow injection–spectrophotometry for the
635 determination of picomolar concentrations of iron in seawater. Limnol Oceanogr
636 -Meth 2:42–54
637 Boyd PW, Watson AJ, Law CS, Abraham ER, Trull T, Murdoch R, Bakker DCE,
638 Bowie AR, Buesseler KO, Chang H, Charette M, Croot P, Downing K, Frew R,
639 Gall M, Hadfield M, Hall J, Harvey M, Jameson G, LaRoche J, Liddicoat M, Ling
640 R, Maldonado MT, McKay RM, Nodder S, Pickmere S, Pridmore R, Rintoul S,
641 Safi K, Sutton P, Strzepek R, Tanneberger K, Turner S, Waite A, Zeldis J (2000) A
642 mesoscale phytoplankton bloom in the polar Southern Ocean stimulated by iron
643 fertilization. Nature 407:695–702
644 Boyd PW, Abraham ER (2001) Iron-mediated changes in phytoplankton photosynthetic
645 competence during SOIREE. Deep-Sea Res II 48:2529–2550
646 Bracher AU, Kroon, BMA, Lucas MI (1999) Primary production, physiological state
647 and composition of phytoplankton in the Atlantic Sector of the Southern Ocean.
648 Mar Ecol Prog Ser 190:1–16
649 Claustre H, Moline MA, Prézelin BB (1997) Sources of variability in the column
650 photosynthetic cross section for Antarctic coastal waters. J Geophys Res 102
651 doi:10.1029/96JC02439
652 Coale KH, Johnson KS, Chavez FP, Buesseler KO, Barber RT, Brzezinski MA,
653 Cochlan WP, Millero FJ, Falkowski PG, Bauer JE, Wanninkhof RH, Kudela RM,

654 Altabet MA, Hales BE, Takahashi T, Landry MR, Bidigare RR, Wang X, Chase Z,
655 Strutton PG, Friederich GE, Gorbunov MY, Lance VP, Hilting AK, Hiscock MR,
656 Demarest M, Hiscock WT, Sullivan KF, Tanner SJ, Gordon RM, Hunter CN, Elrod
657 VA, Fitzwater SE, Jones JL, Tozzi S, Koblizek M, Roberts AE, Herndon J,
658 Brewster J, Ladizinsky N, Smith G, Cooper D, Timothy D, Brown SL, Selph KE,
659 Sheridan CC, Twining BS, Johnson ZI (2004) Southern Ocean iron enrichment
660 experiment: carbon cycling in high- and low-Si waters. Science 304:408–414
661 Cota CF, Smith WO, Mitchell BG (1994) Photosynthesis of *Phaeocystis* in the
662 Greenland Sea. Limnol Oceanogr 39:948–953
663 Cleveland JS, Weidemann AD (1993) Quantifying absorption by aquatic particles: A
664 multiple scattering correction for glass-fiber filters. Limnol Oceanogr 38:1321–
665 1327
666 de Baar HJW, de Jong JTM, Bakker DCE, Löscher BM, Veth C, Bathmann U,
667 Smetacek V (1995) Importance of iron for plankton blooms and carbon dioxide
668 drawdown in the Southern Ocean. Nature 373:412–415
669 de Boyer Montégut C, Madec G, Fischer AS, Lazar A, Iudicone D (2004) Mixed layer
670 depth over the global ocean: An examination of profile data and a profile-based
671 climatology. J Geophys Res 109 doi:10.1029/2004JC002378
672 de Salas MF, Eriksen R, Davidson AT, Wright SW (2011) Protistan communities in the
673 Australian sector of the Sub-Antarctic Zone during SAZ-SENSE. Deep-Sea Res II
674 58:2135–2149
675 Davison IR (1991) Environmental effects on algal photosynthesis: temperature. J
676 Phycol 27:2–8
677 DOE (1994), In: Dickson AG, Goyet C (eds) Handbook of Methods for the Analysis of
678 the Various Parameters of the Carbon Dioxide System in Sea Water, version 2.
679 Carbon Dioxide Information Analysis Center, Report ORNL/ CDIAC-74,
680 OakRidge National Laboratory, OakRidge, Tennessee
681 Dong S, Sprintall J, Gille ST, Talley L (2008) Southern Ocean mixed-layer depth from
682 Argo float profiles. J Geophys Res 113 doi:10.1029/2006JC004051
683 Falkowski PG, Greene RM, Geider RJ (1992) Physiological limitation on
684 phytoplankton productivity in the ocean. Oceanogr 5:84–91
685 Falkowski PG, Green R, Kolber Z (1994) Light utilization and photoinhibition of

686 photosynthesis in marine phytoplankton. In: Baker NR, Bowyer JR (ed)
687 Photoinhibition of photosynthesis: From molecular mechanisms to the field. Bios
688 Scientific
689 Fouilland E, Descolas-Gros C, Courties C, Pons V (1999) Autotrophic carbon
690 assimilation and biomass from size-fractionated phytoplankton in the surface
691 waters across the subtropical frontal zone (Indian Ocean). Polar Biol 21:90–96
692 Gervais F, Riebesell U, Gorbunov MY (2002) Changes in primary productivity and
693 chlorophyll *a* in response to iron fertilization in the Southern Polar Frontal Zone.
694 Limnol Oceanogr 47:1324–1335
695 Goffart A, Catalano G, Hecq JH (2000) Factors controlling the distribution of diatoms
696 and *Phaeocystis* in the Ross Sea. J Marine Syst 27:161–175
697 Gorbunov MY, Kolber ZS, Falkowski PG (1999) Measuring photosynthetic parameters
698 in individual algal cells by Fast Repetition Rate fluorometry. Photosynth Res
699 62:141–153
700 Greene RM, Geider RJ, Kolber Z, Falkowski PG (1992) Iron-induced changes in light
701 harvesting and photochemical energy conversion processes in eukaryotic marine
702 algae. Plant Physiol 100:565–575
703 Hama T, Miyazaki T, Ogawa Y, Iwakuma T, Takahashi M, Otsuki A, Ichimura S
704 (1983) Measurement of Photosynthetic Production of a Marine Phytoplankton
705 Population Using a Stable ^{13}C Isotope. Mar Biol 73:31–36
706 Hirawake T, Satoh H, Ishimaru T, Yamaguchi Y (2000) Photosynthetic characteristics
707 of phytoplankton off Adéieland, Antarctica, during the austral summer. Polar
708 Biosci 13:28–42
709 Hiscok MR, Lance VP, Apprill AM, Bidigare RR, Johnson ZI, Mitchell BG, Smith WO,
710 Barber R (2008) Photosynthetic maximum quantum yield increases are an essential
711 component of the Southern Ocean phytoplankton response to iron. P Natl Acad Sci
712 USA 105:4775–4780
713 Isada T, Kuwata A, Saito H, Ono T, Ishii M, Yoshikawa-Inoue H, Suzuki K (2009)
714 Photosynthetic features and primary productivity of phytoplankton in the Oyashio
715 and Kuroshio-Oyashio transition regions of the northwest Pacific. J Plankton Res
716 31:1009–1025
717 Kishino M, Takahashi M, Okami N, Ichimura S (1985) Estimation of the spectral

718 absorption coefficients of phytoplankton in the sea. Bull Mar Sci 37:634–642
719 Kolber Z, Zehr J, Falkowski P (1988) Effects of growth irradiance and nitrogen
720 limitation on photosynthetic energy conversion in photosystem II. Plant Physiol
721 88:923–929
722 Kolber ZS, Barber RT, Coale KH, Fitzwater SE, Greene RM, Johnson KS, Lindiey S,
723 Falkowski PG (1994) Iron limitation of phytoplankton photosynthesis in the
724 equatorial Pacific Ocean. Nature 371:145–149
725 Korb RE, Whitehouse MJ, Thorpe SE, Gordon M (2005) Primary production across the
726 Scotia Sea in relation to the physico-chemical environment. J Marine Syst 57:231–
727 249
728 Lance VP, Hiscock MR, Hilting AK, Stuebe DA, Bidigare RR, Smith WO, Barber RT
729 (2007) Primary productivity, differential size fraction and pigment composition
730 responses in two Southern Ocean in situ iron enrichments. Deep-Sea Res 54:747–
731 773
732 Lannuzel D, Schoemann V, de Jong J, Tison JL, Chou L (2007) Distribution and
733 biogeochemical behaviour of iron in the East Antarctic sea ice. Mar Chem 106:18–
734 32
735 Latasa M (2007) Improving estimations of phytoplankton class abundances using
736 CHEMTAX. Mar Ecol Prog Ser 329:13–21
737 MacIntyre HL, Geider RJ (1996) Regulation of Rubisco activity and its potential effect
738 on photosynthesis during mixing in a turbid estuary. Mar Ecol Prog Ser 144:247–
739 264
740 Mackey MD, Mackey DJ, Higgins HW, Wright SW (1996) CHEMTAX-a program for
741 estimating class abundances from chemical makers: application to HPLC
742 measurements of phytoplankton. Mar Ecol Prog Ser 144:265–283
743 Marchant HJ, Davidson AT, Wright SW (1987) The distribution and abundance of
744 chroococcoid cyanobacteria in the Southern Ocean. Proc NIPR Symp Polar Biol
745 1:1–9
746 Martin JH, Gordon RM, Fitzwaters SE (1990) Iron in Antarctic waters. Nature
747 345:156–158
748 McNeil BI, Metzl N, Key RM, Matear RJ, Corbiere A (2007) An empirical estimate of
749 the Southern Ocean air-sea CO_2 flux. Global Biogeochem Cy 21:GB3011

750 doi:10.1029/2007GB002991
751 Mitchell BG, Holm-Hansen O (1991) Observations and modeling of the Antarctic
752 phytoplankton crop in relation to mixing depth. Deep-Sea Res 38:981–1007
753 Mitchell BG, Brody EA, Holm-Hansen O, McClain C, Bishop J (1991) Light limitation
754 of phytoplankton biomass and macronutrient utilization in the Southern Ocean.
755 Limnol Oceanogr 36:1662–1677
756 Moline MA, Schofield O, Boucher NP (1998) Photosynthetic parameters and empirical
757 modeling of primary production: a case study on the Antarctic Peninsula shelf.
758 Antarctic Science, 10: 45-54
759 Moore CM, Seeyave S, Hickman AE, Allen JT, Lucas MI, Planquette H, Pollard RT,
760 Poulton AJ (2007) Iron-light interactions during the CROZet natural iron bloom
761 and Export experiment (CROZEX) I: Phytoplankton growth and photophysiology.
762 Deep-Sea Res II 54:2045–2065
763 Nelson DM, Tréguer P (1992) Role of silicon as a limiting nutrient to Antarctic
764 diatoms: evidence from kinetic studies in the Ross Sea ice-edge zone. Mar Ecol
765 Prog Ser 80:255–264
766 Nelson DM, Smith WO (1991) Sverdrup revisited: Critical depths, maximum
767 chlorophyll levels, and the control of Southern Ocean productivity by the
768 irradiance-mixing regime. Limnol Oceanogr 36:1650–1661
769 Odate T, Fukuchi M (1995) Distribution and community structure of picophytoplankton
770 in the Southern Ocean during the late austral summer of 1992. Proc NIPR Symp
771 Polar Biol 8:86–100
772 Orsi AH, Whitworth III T, Nowlin WD (1995) On the meridional extent and fronts of
773 the Antarctic Circumpolar Current. Deep Sea Res 42:641–673
774 Platt T, Gallegos CL, Harrison WG (1980) Photoinhibition of photosynthesis in natural
775 assemblages of marine phytoplankton. J Mar Res 38:687–701
776 Sakshaug E, Bricaud A, Dandonneau Y, Falkowski PG, Kiefer DA, Legendre L, Morel
777 A, Parslow J, Takahashi M (1997) Parameters of photosynthesis: definitions, theory
778 and interpretation of results. J Plankton Res 19:1637–1670
779 Sarmiento JL, Gruber N, Brzezinski MA, Dunne JP (2004) High-latitude controls of
780 thermocline nutrients and low latitude biological productivity. Nature 427:56–60
781 Sarthou G, Timmermans KR, Blain S, Tréguer P (2005) Growth physiology and fate of

782 diatoms in the ocean: a review. J Sea Res 53:25–42
783 Schoemanna V, Becquevorta S, Stefelsb J, Rousseaua V, Lancelot C (2005) *Phaeocystis*
784 blooms in the global ocean and their controlling mechanisms: a review. J Sea Res
785 53:43–66
786 Sedwick PN, Bowie AR, Trull T (2008) Dissolved iron in the Australian sector of the
787 Southern Ocean (CLIVAR SR3 section): Meridional and seasonal trends. Deep-Sea
788 Res 55:911–925
789 Seeyave S, Lucas MI, Moore CM, Poulton AJ (2007) Phytoplankton productivity and
790 community structure in the vicinity of the Crozet Plateau during austral summer
791 2004/2005. Deep-Sea Res II 54:2020–2044
792 Scott FJ, Marchant HJ (2005) Antarctic marine protists. Australian Biological
793 Resources Study and Australian Antarctic Division, p572
794 Smith WO, Asper VL (2001) The influence of phytoplankton assemblage composition
795 on biogeochemical characteristics and cycles in the southern Ross Sea, Antarctica.
796 Deep-Sea Res 48:137–161
797 Sohrin Y, Iwamoto S, Matsui M, Obata H, Nakayama E, Suzuki K, Handa N, Ishii M
798 (2000) The distribution of Fe in the Australian sector of the Southern Ocean.
799 Deep-Sea Res 47:55–84
800 Strutton PG, Griffiths FB, Waters RL, Wright SW, Bindoff NL (2000) Primary
801 productivity off the coast of the East Antarctica (80–150˚E): January to March 1996.
802 Deep-Sea Res II 47:2327–2362
803 Suggett DJ, Moore CM, Hickman AE, Geider RJ (2009) Interpretation of fast repetition
804 rate (FRR) fluorescence: signatures of phytoplankton community structure versus
805 physiological state. Mar Ecol Prog Ser 376:1–19
806 Sukenik A, Bennett J, Falkowski P (1987) Light-saturated photosynthesis – limitation
807 by electron transport or carbon fixation? BBA-Bioenergetics 891:205–215
808 Suzuki K, Kishino M, Sasaoka K, Saitoh S-I, Saino T (1998) Chlorophyll-specific
809 absorption coefficients and pigments of phytoplankton off Sanriku, Northwestern
810 North Pacific. J Oceanogr 54:517–526
811 Suzuki K, Liu H, Saino T, Obata H, Takano M, Okamura K, Sohrin Y, Fujishima Y
812 (2002) East–west gradients in the photosynthetic potential of phytoplankton and
813 iron concentration in the subarctic Pacific Ocean during early summer. Limnol

814 Oceanogr 47:1581–1594
815 Suzuki K, Hinuma A, Saito H, Kiyosawa H, Liu H, Saino T, Tsuda A (2005) Responses
816 of phytoplankton and heterotrophic bacteria in the northwest subarctic Pacific to in
817 situ iron fertilization as estimated by HPLC pigment analysis and flow cytometry.
818 Prog Oceanogr 64:167–187
819 Suzuki K, Saito H, Isada T, Hattori-Saito A, Kiyosawa H, Nishioka J, Michael R,
820 Mckay L, Kuwata A, Tsuda A (2009) Community structure and photosynthetic
821 physiology of phytoplankton in the northwest subarctic Pacific during an in situ
822 iron fertilization experiment (SEEDS-II). Deep-Sea Res II 56:2733–2744
823 Takahashi T, Sutherland SC, Sweeney C, Poisson A, Metzl N, Tilbrook B, Bates N,
824 Wanninkhof R, Feely RA, Sabine C, Olafsson J, Nojiri Y (2002) Global sea-air
825 CO_2 flux based on climatological surface ocean pCO_2, and seasonal biological and
826 temperature effects. Deep-Sea Res II 49:1601–1622
827 Takao S, Hirawake T, Wright SW, Suzuki K (2012) Variations of net primary
828 productivity and phytoplankton community composition in the Indian sector of the
829 Southern Ocean as estimated from ocean color remote sensing data. Biogeosciences,
830 9: 3875–3890
831 Tilzer MM, Elbrächter M, Gieskes WW, Beese B (1986) Light-temperature interactions
832 in the control of photosynthesis in Antarctic phytoplankton. Polar Biol 5:105–111
833 Tomas CR (1997) Identifying Marine Phytoplankton, Academic Press, p858
834 Uitz J, Claustre H, Griffiths FB, Ras J, Garcia N, Sandroni V (2009) A phytoplankton
835 class-specific primary production model applied to the Kerguelen Islands region
836 (Southern Ocean). Deep Sea Res 56:541–560
837 Vaillancourt RD, Sambrotto RN, Green S, Matsuda A (2003) Phytoplankton biomass
838 and photosynthetic competency in the summertime Mertz Glacier Region of East
839 Antarctica. Deep-Sea Res II 50:1415–1440
840 Van Heukelem L, Thomas CS (2001) Computer-assisted high-performance liquid
841 chromatography method development with applications to the isolation and
842 analysis of phytoplankton pigments. J Chromatogr A 910:31–49
843 Van Hilst CM, Smith WO (2002) Photosynthesis/irradiance relationships in the Ross
844 Sea, Antarctica, and their control by phytoplankton assemblage composition and
845 environmental factors. Mar Ecol Prog Ser 226:1–12

Venables H, Moore CM (2010) Phytoplankton and light limitation in the Southern Ocean: Learning from high- nutrient, high-chlorophyll areas. J Geophys Res 115 doi:10.1029/2009JC005361

Welschmeyer NA (1994) Fluorometric analysis of chlorophyll *a* in the presence of Chlorophyll *b* and pheopigments. Limnol Oceanogr 39:1985–1992

Westwood KJ, Griffiths FB, Meiners KM, Williams GD (2010) Primary productivity off the Antarctic coast from 30˚–80˚E; BROKE-West survey, 2006. Deep-Sea Res II 57:794–814

Wright SW, Thomas DP, Marchant HJ, Higgins HW, Mackey MD, Mackey DJ (1996) Analysis of phytoplankton of the Australian sector of the Southern Ocean: comparisons of microscopy and size frequency data with interpretations of pigment HPLC data using the 'CHEMTAX' matrix factorisation program. Mar Ecol Prog Ser 144:285–298

Wright SW, van den Enden RL (2000) Phytoplankton community structure and stocks in the East Antarctic marginal ice zone (BROKE survey, January–March 1996) determined by CHEMTAX analysis of HPLC pigment signatures. Deep-Sea Res II 47:2363–2400

Wright SW, van den Enden RL, Pearce I, Davidson AT, Scott FJ, Westwood KJ (2010) Phytoplankton community structure and stocks in the Southern Ocean (30˚–80˚E) determined by CHEMTAX analysis of HPLC pigment signatures. Deep-Sea Res II 57:758–778

Yoshie N, Suzuki K, Kuwata A, Nishioka J, Saito H (2010) Temporal and spatial variations in photosynthetic physiology of diatoms during the spring bloom in the western subarctic Pacific. Mar Ecol Prog Ser 399:39–52

Yoshikawa T, Meguro M, Takeda S, Furuya K (2007) Spatial heterogeneity in photosynthesis-irradiance parameters of phytoplankton across a cyclonic eddy in the Antarctic Divergence zone along 140˚E. Geophys Res Lett 34 doi:10.1029/2007GL030736

Zapata M, Jeffrey SW, Wright SW, Rodríguez F, Garrido JL, Clementson L (2004) Photosynthetic pigments in 37 species (65 strains) of Haptophyta: implications for oceanography and chemotaxonomy. Mar Ecol Prog Ser 270:83–102

Zubkov MV, Sleigh MA, Tarran GA, Burkill, PH, Leakey RJG (1998) Picoplanktonic

878 community structure on an Atlantic transect from 50˚N to 50˚S. Deep-Sea Res
879 45:1339–1355

880 **Figure Captions**

881

882 **Fig. 1.** Location of sampling stations along 110˚E and 140˚E in the Australian sector of
883 the Southern Ocean. Closed circles and stars represent the stations where seawater was
884 sampled and Photosynthesis–irradiance curve experiments were conducted, respectively.
885 Each line represents the climatological location of one of the four fronts (Orsi et al.,
886 1995): STF, Subtropical Front; SAF, Subantarctic Front; PF, Polar Front; SB, Southern
887 Boundary of the Antarctic Circumpolar Current.

888

889 **Fig. 2.** Contributions of each algal class to the total chl *a* biomass at 5 m estimated by
890 CHEMTAX along (a) 110˚E and (b) 140˚E.

891

892 **Fig. 3.** Changes in the depth of upper mixed layer (z_{UML}) and euphotic zone (z_{eu}),
893 incident surface PAR, and total daily PAR in the upper mixed layer (E_{UML}) along (a, c)
894 110˚E and (b, d) 140˚E.

895

896 **Fig. 4.** Changes in the photosynthetic parameters at 5 m along 110˚E and 140˚E: (a)
897 maximum photosynthetic rate (P^*_{max}: mg C (mg chl *a*)$^{-1}$ h^{-1}), (b) initial slope of the *P*–*E*
898 curve (α^*: [mg C (mg chl *a*)$^{-1}$ h^{-1}] (μmol photons m^{-2} s^{-1})$^{-1}$), (c) photoinhibition index
899 (β^*: [mg C (mg chl *a*)$^{-1}$ h^{-1}] (μmol photons m^{-2} s^{-1})$^{-1}$), (d) maximum quantum yield of
900 carbon fixation ($\Phi_{c\ max}$: mol C (mol photons)$^{-1}$), (e) mean chl *a*-specific absorption

coefficient of phytoplankton ($\bar{a}^*_{\varphi}$: m^2 (mg chl a)$^{-1}$), and (f) light saturation index (E_k: µmol photons m^{-2} s^{-1}) in the study area.

Fig. 5. Relationship between the photochemical quantum efficiency (F_v/F_m) and the functional absorption cross-section (σ_{PSII}) of photosystem II for the phytoplankton community at 5 m along 110˚E and 140˚E.

Fig. 6. Temporal and spatial changes in the distributions of satellite-derived chl *a* concentration in the study area from August 2010 to March 2011 along (a) 110˚E and (b) 140˚E. Data points were extracted with 3 × 3 pixels (i.e., 27 km × 27 km) resolution from MODIS/Aqua 8-day composite images. Areas in white represent lack of satellite data due to sea-ice cover and/or cloudiness. Arrows indicate sampling stations in Fig. 1.

Fig. 7. Light microscopy images of the pennate diatom *Fragilariopsis kerguelensis* with chains: (a) D14 (b) D15. The black bar in the images is 20 µm.

Table 1. CHEMTAX analysis of accessory pigment to chl *a* ratios in the major algal class: (a) initial ratios and (b) final ratios. Perid, peridinin; 19'-But, 19'-butanoyloxyfucoxanthin; Fucox, fucoxanthin; 19'-Hex, 19'-hexanoyloxyfucoxanthin; Neox, neoxanothin; Prasinox, prasinoxanthin; Violax, violaxanthin; Allox, alloxanthin; Chl *b*, chlorophyll *b*; Chl *a*, chlorophyll *a*.

	Perid	19'-But	Fucox	19'-Hex	Neox	Prasinox	Violax	Allox	Zeax	Chl *b*	Chl *a*
(a)											
Prasinophytes	0	0	0	0	0.039	0.069	0.097	0	0	2.235	1
Dinoflagellates	0.781	0	0	0	0	0	0	0	0	0	1
Cryptophytes	0	0	0	0	0	0	0	0.118	0	0	1
Haptophytes6	0	0.041	0.112	0.957	0	0	0	0	0	0	1
Haptophytes8	0	0.327	0.069	0.613	0	0	0	0	0	0	1
Chlorophytes	0	0	0	0	0.003	0	0.01	0	0.003	0.006	1
Cyanobacteria	0	0	0	0	0	0	0	0	0.507	0	1
Diatoms	0	0	0.664	0	0	0	0	0	0	0	1
(b)											
Prasinophytes	0	0	0	0	0.039	0.067	0.097	0	0	2.235	1
Dinoflagellates	0.781	0	0	0	0	0	0	0	0	0	1
Cryptophytes	0	0	0	0	0	0	0	0.118	0	0	1
Haptophytes6	0	0.043	0.117	1.398	0	0	0	0	0	0	1
Haptophytes8	0	0.327	0.069	0.613	0	0	0	0	0	0	1
Chlorophytes	0	0	0	0	0.003	0	0.01	0	0.003	0.006	1
Cyanobacteria	0	0	0	0	0	0	0	0	0.507	0	1
Diatoms	0	0	0.664	0	0	0	0	0	0	0	1

Table 2. Summary of hydrographic conditions and phytoplankton abundance along 110˚E and 140˚E. SST: sea surface temperature (°C), SSS: sea surface salinity, N: nitrate (= nitrate + nitrite) concentration (μmol L^{-1}), P: phosphate concentration (μmol L^{-1}), Si: silicate concentration (μmol L^{-1}), chl *a*: chlorophyll *a* concentration, chl a_{micro}: chlorophyll *a* concentration by micro-sized (>20 μm) phytoplankton, micro-size contribution: ratio of chl a_{micro} to chl *a* (%).

Station	Date	Latitude (°S)	Longitude (°E)	SST (°C)	SSS	N (μmol L^{-1})	P (μmol L^{-1})	Si (μmol L^{-1})	*Synechococcus* ($\times 10^3$ cells ml^{-1})	chl *a* (mg m^{-3})	chl a_{micro} (mg m^{-3})	Micro-size contribution (%)
110°E												
C01	26 Dec 2010	40.0	110.0	14.8	35.2	1.72	0.31	0.00	28.5	0.30	0.00	0.0
S02	26 Dec 2010	41.0	110.0	15.9	35.3	0.58	0.24	0.00	21.5	0.47	0.01	1.4
S03	26 Dec 2010	43.3	110.0	13.3	34.7	6.96	0.62	0.17	2.5	0.68	0.09	13.4
C02	26 Dec 2010	45.0	110.0	11.3	34.5	11.32	0.93	0.00	2.0	0.18	0.00	0.0
S05	27 Dec 2010	47.6	110.0	9.6	34.2	17.67	1.26	1.70	1.4	0.18	0.00	0.0
C03	28 Dec 2010	50.0	110.0	8.0	33.9	22.59	1.64	6.70	0.5	0.19	0.00	2.4
S06	28 Dec 2010	51.6	110.2	4.6	33.9	24.93	1.85	10.05	0.3	0.40	0.04	10.6
C04	29 Dec 2010	55.0	110.0	5.0	33.9	26.41	1.97	23.21	0.2	0.49	0.06	12.9
C05	30 Dec 2010	58.4	110.0	3.1	33.9	26.46	1.82	24.42	0.2	0.37	0.15	39.0
C06	31 Dec 2010	60.0	110.0	2.2	33.9	26.09	1.84	29.21	0.2	0.65	0.28	42.6
S09	1 Jan 2011	62.1	109.9	1.3	33.4	23.30	1.64	36.81	0.2	0.99	0.25	24.8
C08	1 Jan 2011	63.0	110.0	1.2	33.3	22.10	1.36	37.80	0.2	0.78	0.14	18.4
C10	2 Jan 2011	65.0	110.0	2.6	33.8	21.17	1.25	52.52	0.2	0.57	0.05	7.9
C17	4 Jan 2011	63.0	115.0	2.0	33.7	23.17	1.59	34.70	0.2	0.67	0.12	17.2
140°E												
S15	9 Jan 2011	66.0	140.4	0.7	33.9	26.08	1.85	54.53	0.2	0.69	0.06	8.4
D07	10 Jan 2011	65.0	140.0	0.9	33.6	26.74	1.90	47.09	0.2	0.27	0.02	7.3
D08	11 Jan 2011	64.0	140.1	1.7	33.5	26.30	1.81	40.78	0.2	0.26	0.01	4.8
D10	14 Jan 2011	62.5	140.0	1.7	33.7	24.57	1.77	30.82	0.2	0.92	0.46	49.7
D12	15 Jan 2011	60.0	140.0	2.5	33.9	26.31	1.75	20.59	0.2	0.30	0.02	8.1
D13	16 Jan 2011	58.6	140.0	4.8	33.7	24.67	1.78	3.04	0.3	0.34	0.06	16.5
S21	16 Jan 2011	57.0	140.0	4.8	33.7	22.77	1.53	2.23	0.2	0.32	0.10	29.9
D14	17 Jan 2011	55.0	140.0	5.0	33.8	23.92	1.68	0.18	0.2	0.31	0.13	43.0
D15	18 Jan 2011	50.0	143.7	10.0	34.1	17.36	1.28	0.00	1.6	0.30	0.00	0.0

Table 3. Nonparametric Kendall's rank correlations between photosynthetic parameters and the diatom contribution to the chl *a* biomass (n = 11). P^*_{max}: maximum photosynthetic rate (mg C (mg chl *a*)$^{-1}$ h^{-1}), α^*: initial slope of the *P*–*E* curve ([mg C (mg chl *a*)$^{-1}$ h^{-1}] (μmol photons m^{-2} s^{-1})$^{-1}$), β^*: photoinhibition index ([mg C (mg chl *a*)$^{-1}$ h^{-1}] (μmol photons m^{-2} s^{-1})$^{-1}$),$\Phi_{c\,max}$: maximum quantum yield of carbon fixation (mol C (mol photons)$^{-1}$), $\bar{a}^*_{\varphi}$: mean chl *a*-specific absorption coefficient of phytoplankton (m^2 (mg chl *a*)$^{-1}$), E_k: light saturation index (μmol photons m^{-2} s^{-1}), F_v/F_m: photochemical quantum efficiency of photosystem II, σ_{PSII}: functional absorption cross-section of photosystem II (×10^{-20} m^2 photon^{-1}), Diatom contribution: diatom contribution to the chl *a* biomass.

	P^*_{max}	α^*	β^*	$\Phi_{c\,max}$	$\bar{a}^*_{\Phi}$	E_K	F_v/F_m	σ_{PSII}
α^*	**0.71** **							
β^*	**0.49** *	0.42						
$\Phi_{c\,max}$	**0.64** **	**0.71** **	**0.56** *					
$\bar{a}^*_{\Phi}$	-0.05	-0.50	0.42	-0.35				
E_K	-0.09	-0.38	0.05	-0.24	-0.13			
F_v/F_m	-0.09	0.05	**-0.54** *	-0.09	0.35	-0.17		
σ_{PSII}	0.20	0.13	0.20	0.05	0.09	0.20	-0.28	
Diatom contribution	**0.53** *	0.45	**0.75** ***	**0.67** **	**-0.53** *	-0.05	-0.28	0.09

Bold numbers denote statistical significance; *0.01<P≦0.05, **0.001<P≦0.01,***P≦0.001.

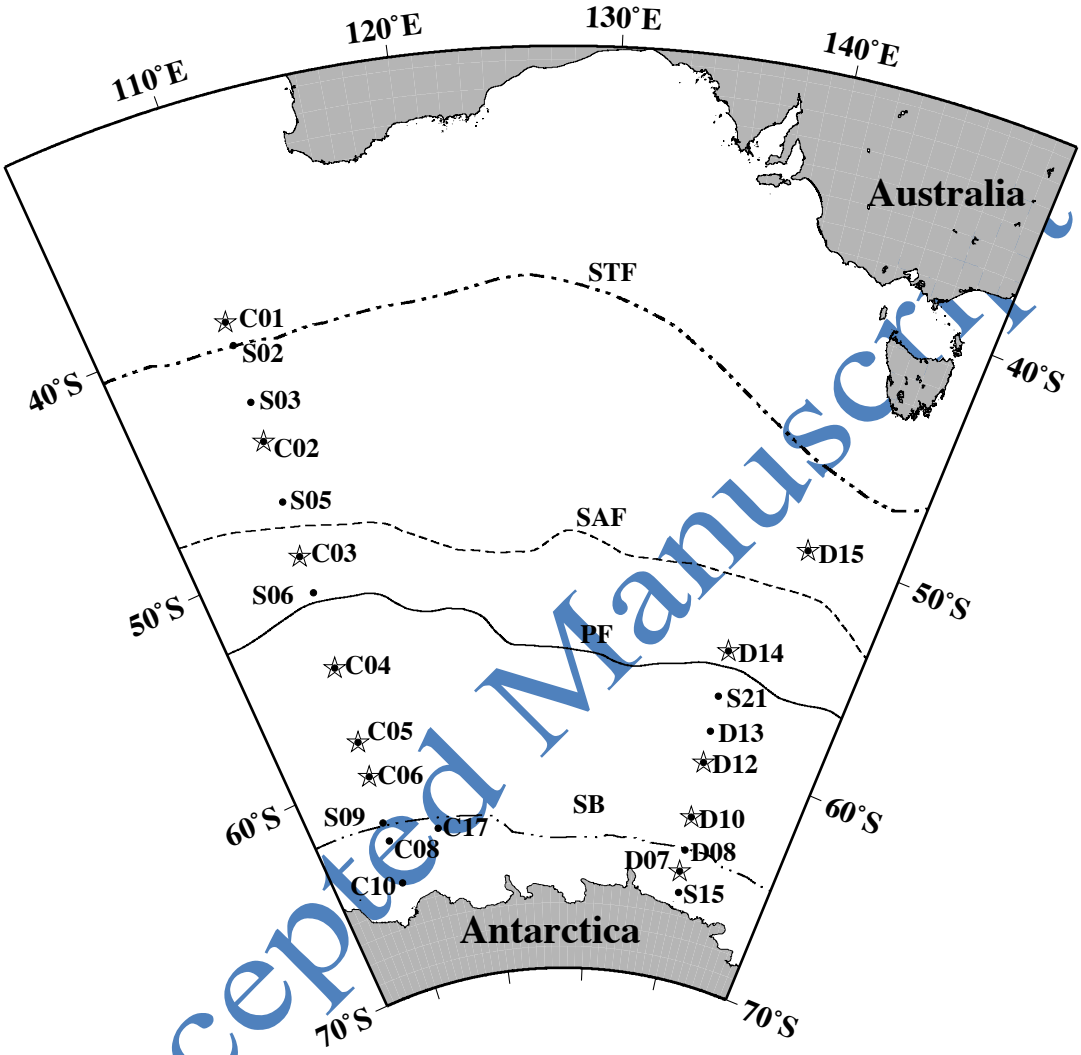

Takao et al. Figure 1

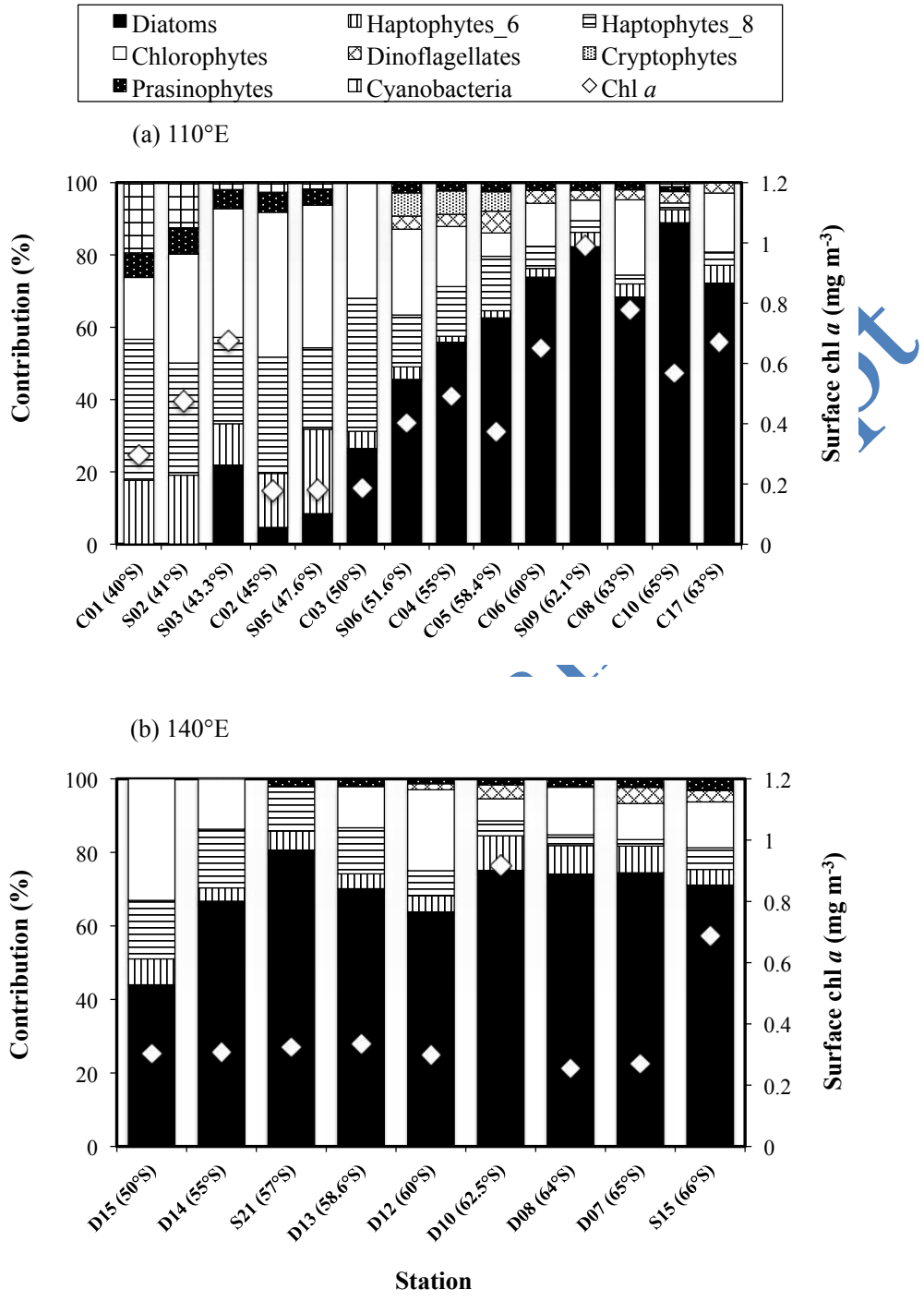

Takao et al. Figure 2

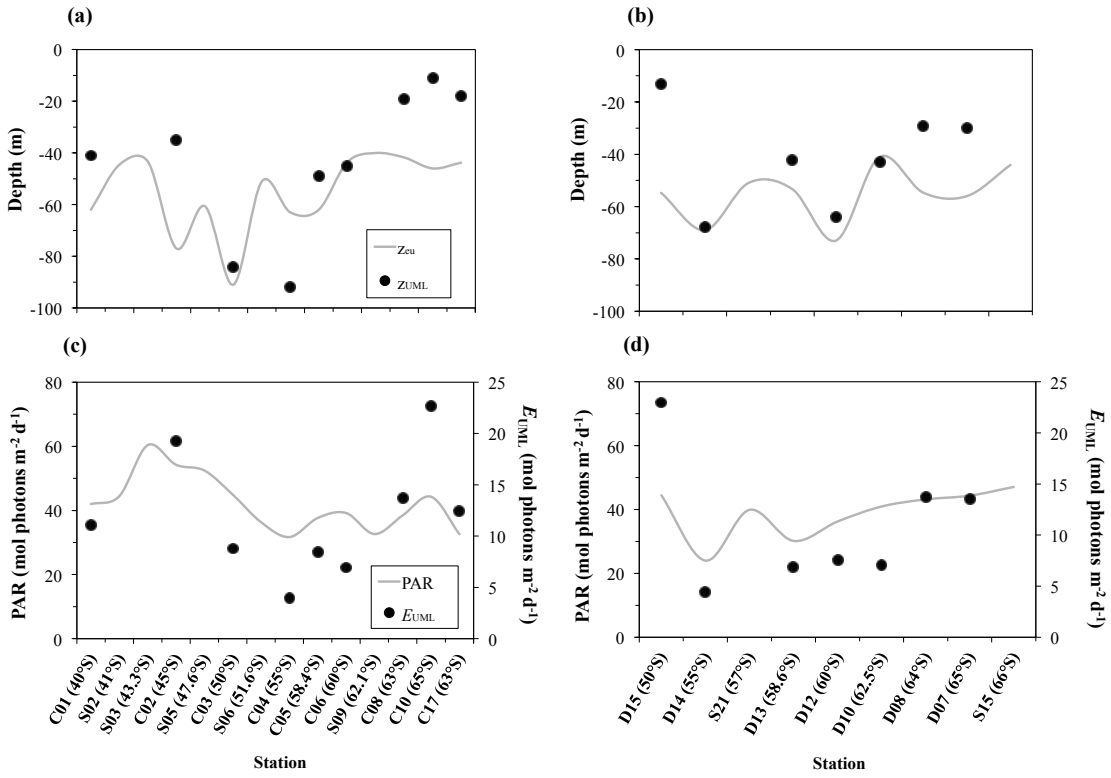

Takao et al. Figure 3

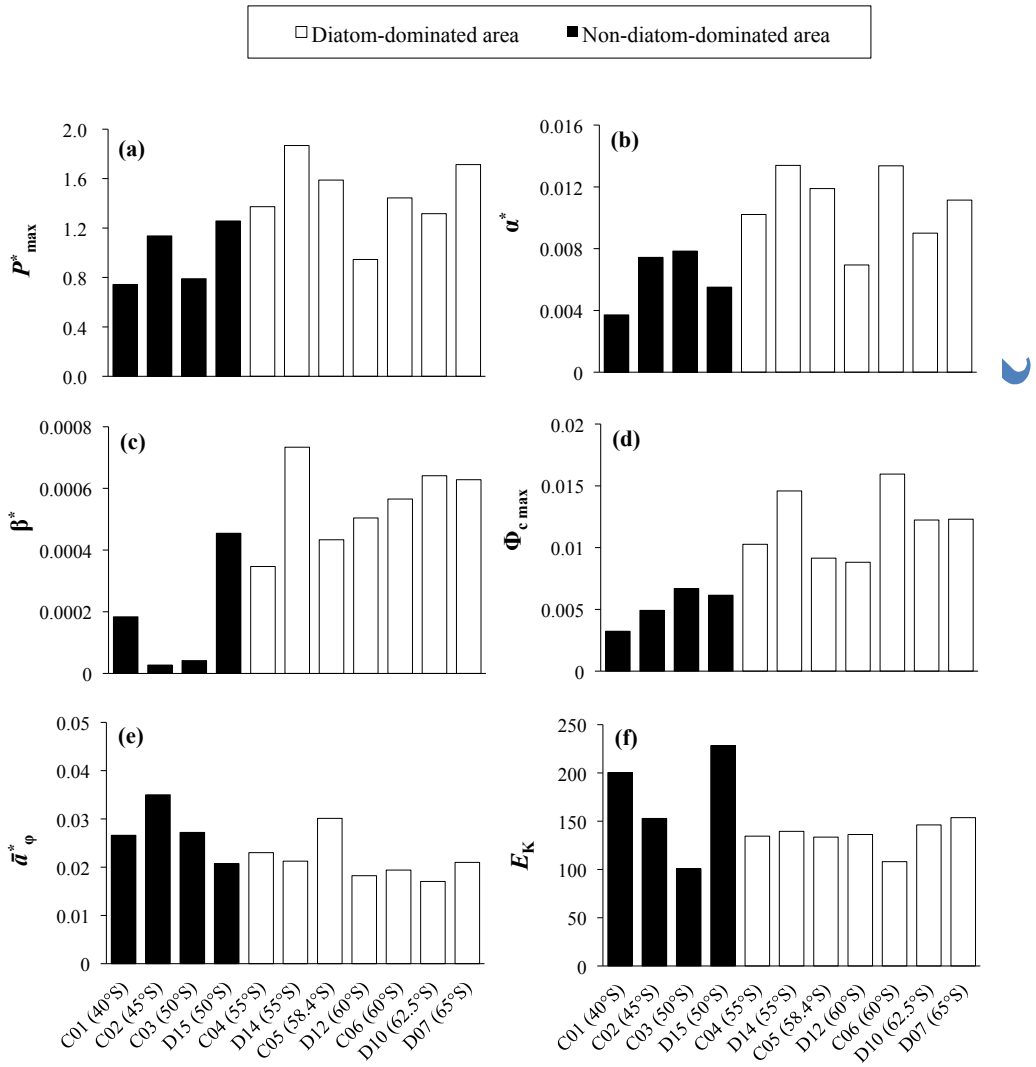

Takao et al. Figure 4

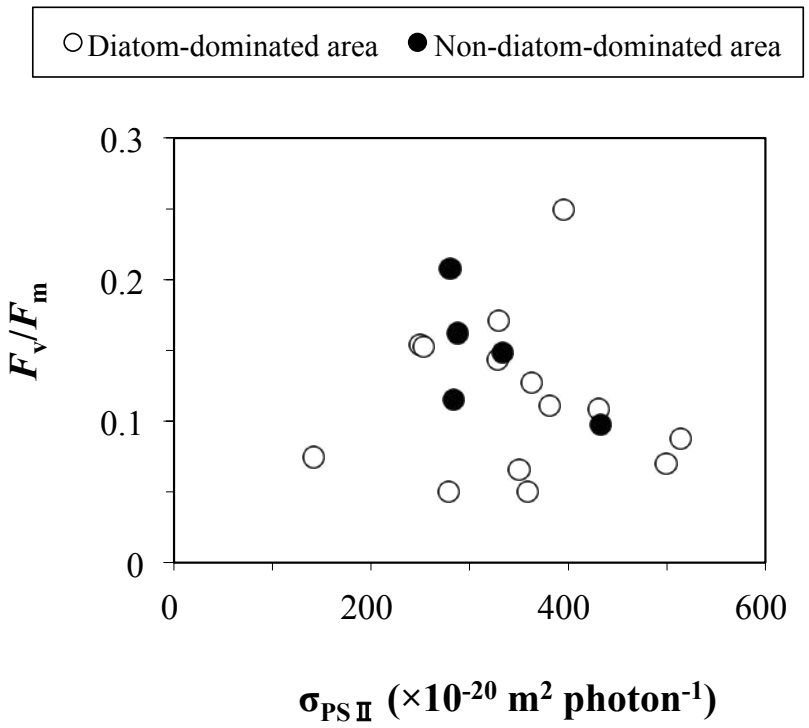

Takao et al. Figure 5

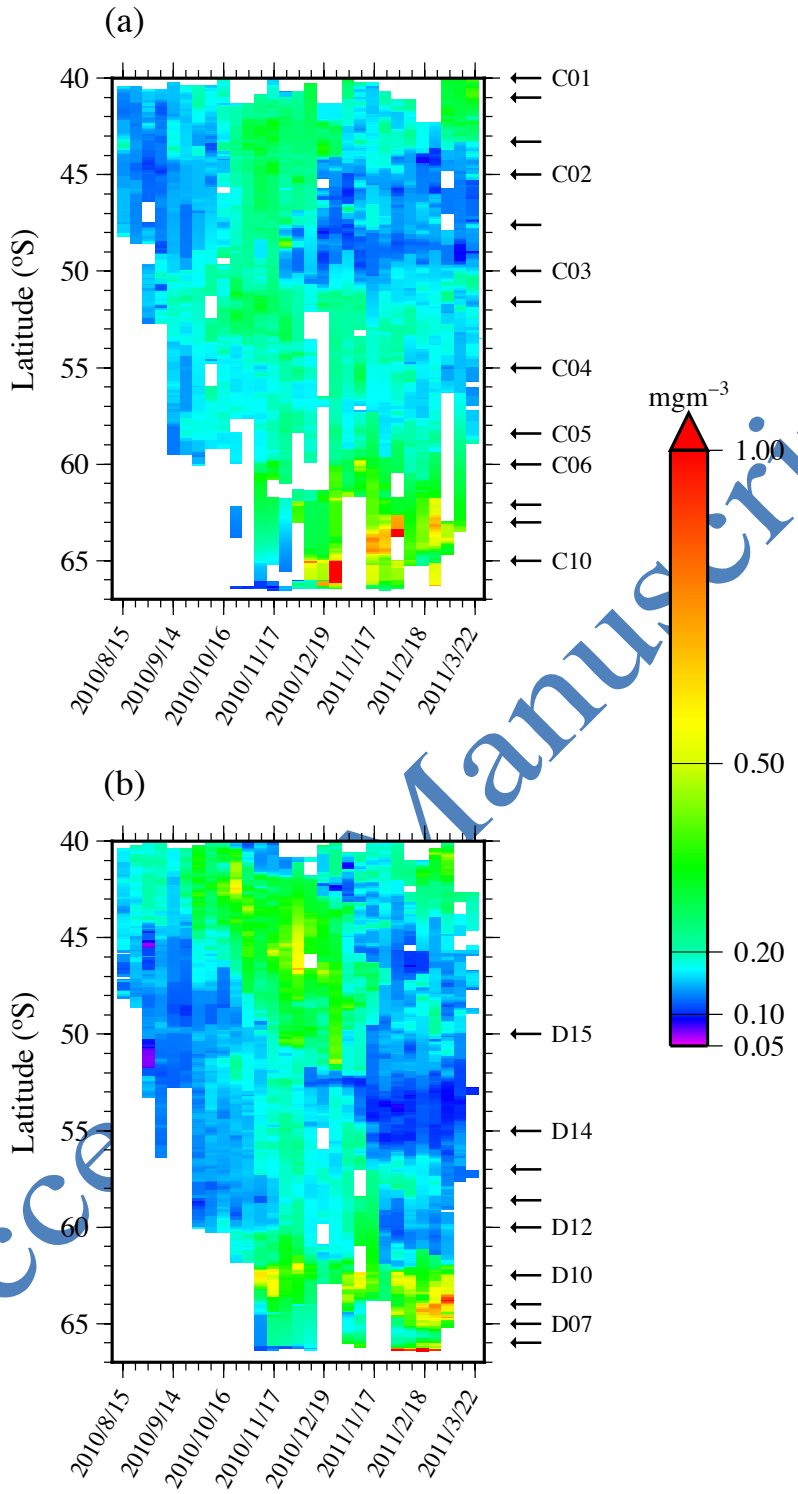

Takao et al. Figure 6

(a)

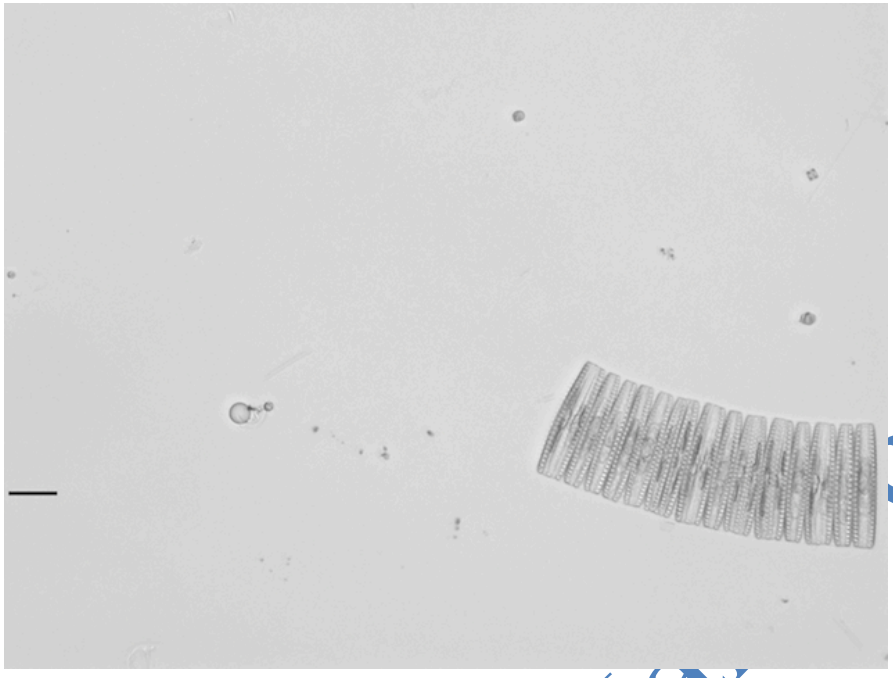

(b)

Takao et al. Figure 7